energies

MDPI

Article

Inter-Zone Optimal Scheduling of Rural Wind–Biomass-Hydrogen Integrated Energy System

Mingguang Zhang, Shuai Yu * and Hongyi Li

College of Electrical and Information Engineering, Lanzhou University of Technology, Lanzhou 730050, China; zhangmg@lut.edu.cn (M.Z.); 212085800078@lut.edu.cn (H.L.)
* Correspondence: 212080802008@lut.edu.cn

Abstract: To solve the problems of low utilization of biomass and uncertainty and intermittency of wind power (WP) in rural winter, an interval optimization model of a rural integrated energy system with biogas fermentation and electrolytic hydrogen production is constructed in this paper. Firstly, a biogas fermentation kinetic model and a biogas hydrogen blending model are developed. Secondly, the interval number is used to describe the uncertainty of WP, and an interval optimization scheduling model is developed to minimize daily operating cost. Finally, a rural integrated energy system in Northeast China is taken as an example, and a sensitivity analysis of electricity price, gas production, and biomass price is conducted. The simulation results show that the proposed strategy can significantly reduce the wind abandonment rate and improve the economy by 3.8–22.3% compared with conventional energy storage under optimal dispatch.

Keywords: WP; rural integrated energy system; biogas fermentation; uncertainty

check for updates

Citation: Zhang, M.; Yu, S.; Li, H. Inter-Zone Optimal Scheduling of Rural Wind–Biomass-Hydrogen Integrated Energy System. *Energies* **2023**, *16*, 6202. https://doi.org/10.3390/en16176202

Received: 12 July 2023
Revised: 5 August 2023
Accepted: 16 August 2023
Published: 26 August 2023

Copyright: © 2023 by the authors. Licensee MDPI, Basel, Switzerland. This article is an open access article distributed under the terms and conditions of the Creative Commons Attribution (CC BY) license (https://creativecommons.org/licenses/by/4.0/).

1. Introduction

With the world's energy crisis and environmental pollution and other problems becoming increasingly prominent, a comprehensive energy system with clean energy as the mainstay has gradually become the main direction of low-carbon development in countries around the world. Biomass has received a lot of attention because of its abundant resources and huge carbon reduction potential [1–3]. However, the low production of rural biogas in winter [4] and uncontrollable renewable energy sources pose challenges to the optimal dispatch of integrated rural energy systems.

Problems such as intermittency of renewable energy and mismatch of grid construction increase the abandonment rate of renewable energy [5], so studying the role of various forms of energy storage in an integrated energy system is an effective way to cope with it. Song et al. [6] propose that battery energy storage systems combined with renewable energy generation can solve the intermittency problem of renewable energy generation to smooth out output fluctuations. Wu et al. [7] developed an integrated energy system scheduling model which contains multiple types of electrical, thermal, and hydrogen energy storage devices. Karaca et al. [8] proposed the storage of excess power from scenic output through a compressed air energy storage system. Liu et al. [9] investigate the role of pumped storage power plants and hydrogen storage in urban carbon reduction. Siddiqui et al. [10] evaluated the energy output potential of ammonia storage. In existing studies, energy storage is mostly carried out in the form of traditional chemical storage or mechanical storage, and few studies have investigated thermal storage and release characteristics of biogas digesters.

The addition of energy storage can provide a solution for the coordinated optimization of integrated energy systems, but the high price of energy storage limits the development of renewable energy and storage co-generation systems, so studying the complementary characteristics between renewable energy sources can reduce the dependence of integrated energy systems on energy storage. Xu et al. [11] established a mixed integer nonlinear

programming model containing geothermal, solar, and wind energy. Li et al. [12] considered the complementary characteristics between biomass and solar energy to provide a solution for the effective operation of the isolated integrated energy system. Zhou et al. [13] fully considered the intermittent nature of the WP output and the stability of the biomass power output, and the simulation results show that the proposed model can operate economically on typical days in summer and winter. However, the complementary characteristics between wind, biogas, and hydrogen have been less studied.

The feasibility and effectiveness of multi-fuel combustion mixtures have been studied. Zare et al. [14] explored the optimal mixing ratio of biogas and natural gas. Zhao et al. [15] proposed an ammonia-coal co-firing technology with a view of reducing the total operating cost. Kim et al. [16] explored the economics of mixing hydrogen and natural gas for power generation. Zhang et al. [17] studied the energy efficiency of co-firing coal and different kinds of biomass. Multi-fuel blending will provide new options for integrated energy system operation.

In summary, this paper integrates the complementary characteristics of wind energy, biogas, and hydrogen and the energy time-shifting characteristics of energy storage and establishes an integrated rural energy system model considering biogas fermentation and biogas and hydrogen mixing, while introducing interval optimization [18–20] to solve the uncertainty problem of WP. Interval optimization can well reflect the influence from uncertainty, unlike robust optimization [21,22], which only describes the worst case. The main contributions of this paper are the following:

(1) The heat storage and discharge characteristics of the biogas digester (BD) are studied, and the uncertainty of WP output is expressed in the form of interval numbers, and the optimization objective takes into account the economy and carbon reduction.
(2) The interval model is transformed into a mixed integer linear programming model with optimal and worst solutions and is resolved using an interval linear programming algorithm.
(3) The economic and environmental benefits of using conventional energy storage and the strategy proposed in this paper are compared, and a sensitivity analysis of biomass price, electricity price, and gas production is conducted.

2. Integrated Rural Energy System Model

The architecture of the integrated electrical and thermal energy system is shown in Figure 1, which contains electricity, heat, hydrogen, and biomass energy streams. WP is the main high-power equipment to meet the daytime electricity load, and the energy conversion devices micro gas turbine (MT) and heat pump (HP) meet the daytime thermal load. The electrolyzer (EL) dissipates WP to store hydrogen at the peak of WP output at night, and at the peak of electrical load hydrogen and biogas enter the MT to generate electricity. The BD has a similar role as a heat storage tank, storing heat when the system generates excess heat to keep the BD warm and, thus, increase biogas production. The addition of the hydrogen storage tank (HST) and biogas storage tank (BST) allows the energy to be discharged at peak load level. Accordingly, the system achieves a coupling between electric heat and biogas and hydrogen.

2.1. BD

Biogas fermentation is mainly affected by temperature, and changing the temperature of the feed solution can change the gas production rate [23]. In this paper, medium temperature fermentation was used, with temperature variation ranging from 10 °C to 30 °C. The effect of other external factors on the digester was ignored, and the relationship between biogas production and temperature of the digester was used as follows:

$$E_{bio} = aT_{liq} + b \quad (1)$$

where T_{liq} is the actual reaction temperature. a, b are the coefficient obtained from data fitting. E_{bio} is the BD unit time yield.

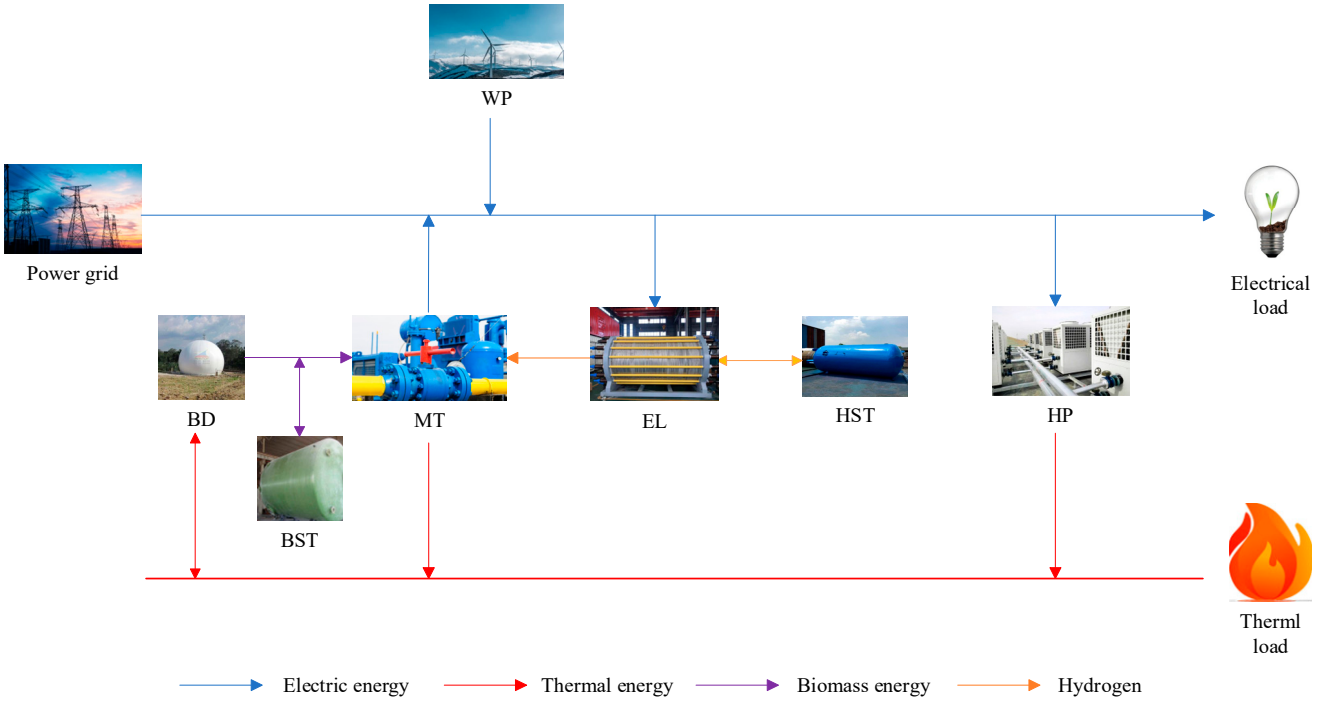


Figure 1. The architecture of the integrated electrical and thermal energy system.

Considering that the density and specific heat capacity of the feed liquid is close to water, the capacity of storing heat is large, so, to a certain extent, the BD is used as a heat storage device, and the heat exchange is used to achieve the consumption and supply of heat energy to the system.

The temperature variation of biogas fermentation satisfies:

$$T_{liq}(t) = T_{liq}(t-1) + \frac{\left[P_{mg,h}(t) - P_{dis,mg,h}(t)\right]}{C_{liq}\rho_{liq}V_{mg}} \tag{2}$$

$$P_{mg,h}(t) = \eta_{mg}P_{c,mg,h}(t) - \frac{P_{d,mg,h}(t)}{\eta_{mg}} \tag{3}$$

$$P_{dis,mg,h}(t) = \delta_{dis}S_{mg}\left[T_{liq}(t) - T_{am}(t)\right] \tag{4}$$

where $P_{mg,h}$ and $P_{dis,mg,h}$ are the fermenter heating and cooling power. C_{liq}, ρ_{liq}, V_{mg} are the specific heat capacity, density, and volume of the liquid. $P_{c,mg,h}$ and $P_{d,mg,h}$ are the fermenter charging and discharging power. η_{mg} is the charging and discharging efficiency. δ_{dis}, S_{mg} are the fermenter surface heat transfer coefficient and heat dissipation area. T_{am} is the ambient temperature.

2.2. Hydrogen Doping Model for Biogas

By mixing up to 50% of hydrogen in biogas, the burner can meet the stability requirements and improve the system efficiency [24,25]. The mathematical model of MT hydrogen doping is as follows:

$$P_e^{MT} = \eta_{MT,e}(P_{CH_4}^{MT} + P_{H_2}^{MT}) \tag{5}$$

$$P_h^{MT} = \eta_{MT,h}P_e^{MT} \tag{6}$$

where P_e^{MT} and P_h^{MT} are the electrical and thermal power output of the MT at t. $P_{CH_4}^{MT}$, $P_{H_2}^{MT}$ are the power input of biogas and hydrogen to the MT. $\eta_{MT,e}$ and $\eta_{MT,h}$ are the electrical power and thermoelectric ratio of the MT.

2.3. WP Uncertainty

There is a large relationship between WP output and wind speed, but the wind speed is not controllable, so the uncertainty of WP output is described using the interval number [26], which is expressed as:

$$\left[P_{wp}(t)\right] = \left[P_{wp}^{-}(t), P_{wp}^{+}(t)\right] \tag{7}$$

where $P_{wp}(t)$ indicates the WP output at the time of t. $P_{wp}^{-}(t)$, $P_{wp}^{+}(t)$ indicate the lower and upper limits of WP output.

The WP uncertainty is mainly due to the wind speed prediction error, and in the subsequent analysis, the interval number operation is used as the basis, so the following equation can also be expressed:

$$\left[P_{wp}(t)\right] = \left[P_{wpre}(t) - n \cdot P_{wpre}(t), P_{wpre,t}(t) + n \cdot P_{wpre}(t)\right] \tag{8}$$

where $P_{wpre}(t)$ is the predicted WP output. n is the prediction error.

3. Optimization Model for Day-Ahead Dispatching of Electric and Thermal Rural Integrated Energy Systems

3.1. Objective Function

The objective function is the lowest daily operating cost. The total operating costs include power purchase costs, maintenance costs, feedstock costs, and wind abandonment costs, and the benefits are derived from the carbon reduction benefits generated by replacing fossil fuel combustion with biogas [27]:

$$\min C_{total} = C_{ele} + C_{om} + C_{rm} + C_{aba} + C_{co_2} \tag{9}$$

Among them:

$$C_{ele} = \sum_{t=1}^{T} \lambda_{ele} P_{buy,e}(t) \tag{10}$$

$$C_{om} = \sum_{t=1}^{T} \lambda_{j,yw} P_{j,t}(t) \tag{11}$$

$$C_{rm} = \sum_{t=1}^{T} \lambda_g P_g^{AD}(t) \tag{12}$$

$$C_{aba} = \sum_{t=1}^{T} \lambda_{wind} P_{aba,e}(t) \tag{13}$$

$$C_{co_2} = \lambda_{co_2} \left[\alpha \eta_{MT,e} \sum_{i=1}^{24} P_{CH_4}^{MT}(t) + \beta \eta_{MT,h} \sum_{i=1}^{24} P_{CH_4}^{MT}(t) \right] \tag{14}$$

where C_{total} is the total operating cost of the system. C_{ele} is the power purchase cost. C_{om} is the maintenance cost. C_{rm} is the raw material cost. C_{aba} is the wind abandonment cost. C_{co_2} is the carbon emission reduction benefit. λ_{ele} is the electricity price. $P_{buy,e}$ is the power purchased from the grid in the period of t. $\lambda_{j,yw}$ is the unit maintenance cost of the equipment j. $P_{j,t}$ is the output of the equipment j in the period of t. λ_g is the biogas production cost per unit power. P_g^{AD} is the gas production power of the BD. λ_{wind} is the wind abandonment penalty factor. $P_{aba,e}$ is the abandoned power of the wind turbine in

the period of t. λ_{co_2} is the carbon trading price. α and β are the carbon emission factor of electricity and the carbon emission factor of natural gas.

3.2. Constraints

3.2.1. Power Balance Constraint

(1) Electrical power balance

$$\left[P_{wp}(t)\right] + P_e^{MT}(t) + P_{buy,e}(t) - P_e^{HP}(t) - P_e^{EL}(t) - P_{aba,e}(t) = P_{Load,e}(t) \tag{15}$$

where $P_e^{HP}(t)$ is the electrical power of the HP. $P_e^{EL}(t)$ is the electrical power of the EL. $P_{Load,e}(t)$ is the electrical load.

(2) Thermal power balance

$$P_h^{MT}(t) + P_h^{HP}(t) - P_{mg,h}(t) = P_{Load,h}(t) \tag{16}$$

where $P_h^{HP}(t)$ is the HP heat production power. $P_{Load,h}(t)$ is the heat load.

(3) Gas flow rate equilibrium

$$P_g^{EL}(t) + P_d^{HST}(t) - P_c^{HST}(t) - P_{H_2}^{MT}(t) = 0 \tag{17}$$

$$P_g^{AD}(t) + P_d^{BST}(t) - P_c^{BST}(t) - P_{CH_4}^{MT}(t) = 0 \tag{18}$$

where $P_g^{EL}(t)$ is the EL gas production power. $P_c^{HST}(t)$, $P_d^{HST}(t)$ are the HST charging and discharging power. $P_d^{BST}(t)$, $P_c^{BST}(t)$ are the BST charging and dis-charging power.

3.2.2. Equipment Constraints

(1) Energy conversion equipment constraints

$$P_{N,\min} \le P_N(t) \le P_{N,\max} \tag{19}$$

where $N \in \{MT, EL, HP\}$. $P_{N,\max}$ and $P_{N,\min}$ are the equipment power's upper and lower limits.

(2) The energy storage charging and discharging constraints are:

$$0 \le Q_{c,f}(t) \le Q_{c,f,\max} k_{c,f} \tag{20}$$

$$0 \le Q_{d,f}(t) \le Q_{d,f,\max} k_{d,f} \tag{21}$$

$$0 \le k_{c,f} + k_{d,f} \le 1 \tag{22}$$

$$S_{f,\min} \le S_f(t) \le S_{f,\max} \tag{23}$$

where $Q_{c,f,\max}$ and $Q_{d,f,\max}$ are the maximum filling and discharging thermal power of BD and the maximum filling and discharging rate of HST and BST. $k_{c,f}, k_{d,f} \in \{0,1\}$ indicate the filling and discharging status. $S_{f,\min}$ and $S_{f,\max}$ are the minimum and maximum temperature of BD and the minimum and a maximum capacity of HST and BST.

4. Interval Optimization Model and Solution Algorithm

4.1. Interval Optimization Model

The interval optimization problem proposed in this paper can be summarized in the following form:

$$\begin{cases} \min C_{total}^{I}(X, U, P_{wp}^{\pm}) \\ s.t.(15)-(18),(19)-(23) \\ X \in \Omega^{n} \end{cases} \tag{24}$$

where X is the N-dimensional decision vector. U is the uncertainty of the system parameters. $P_{wp}^{\pm}$ is the uncertainty interval matrix of the WP output. Ω^{n} is the range of X. The constraint Equations (15)–(18) and (19)–(23) are the equation constraints and inequality constraints.

In the model of the integrated wind-methane hydrogen storage energy system, for any of the decision variable matrices X and U in Equation (24), the range of values of the objective function $C_{total}^{I}(X, U, P_{wp}^{\pm})$ under the influence of the uncertainty vector matrix $P_{wp}^{\pm}$ is:

$$C_{total}^{I}(X, U) = [C_{total}^{L}(X, U), C_{total}^{R}(X, U)] \tag{25}$$

where $C_{total}^{L}(X, U)$ is the lower limit of the interval. $C_{total}^{R}(X, U)$ is the upper limit of the interval.

Since in engineering, the midpoint value of the interval represents the average expected level of the system under the influence of uncertain parameters, and the radius of the interval represents the level of system variation under the influence of uncertain parameters, the interval of the range of values of the objective function $C_{total}^{I}(X, U, P_{wp}^{\pm})$ can be further expressed as [28]:

$$C_{total}^{I}(X, U) = [C_{total}^{C}(X, U), C_{total}^{W}(X, U)] \tag{26}$$

$$C_{total}^{C}(X, U) = \frac{C_{total}^{L}(X, U) + C_{total}^{R}(X, U)}{2} \tag{27}$$

$$C_{total}^{W}(X, U) = \frac{C_{total}^{R}(X, U) - C_{total}^{L}(X, U)}{2} \tag{28}$$

where $C_{total}^{C}(X, U)$ is the midpoint value of the interval of the objective function. $C_{total}^{W}(X, U)$ is the radius of the interval of the objective function.

4.2. Solution Algorithm

Considering the uncertainty of WP, the interval linear optimization method is used to resolve the day-ahead dispatch modelling of integrated rural energy systems, and the optimal sub-model and the worst sub-model are constructed instead of the original interval optimization model [18]. The optimal sub-model represents the deterministic model obtained when the WP is maximum, and the worst sub-model represents the deterministic model obtained when the WP output is minimum. Finally, MATLAB+Cplex is used to solve the model and obtain the operating strategy for the day-ahead dispatch of the integrated rural energy system, including the range of equipment output and power consumption scheme, as well as the range of operating costs of the system. The interval linear optimization solution algorithm flow is shown in Figure 2.

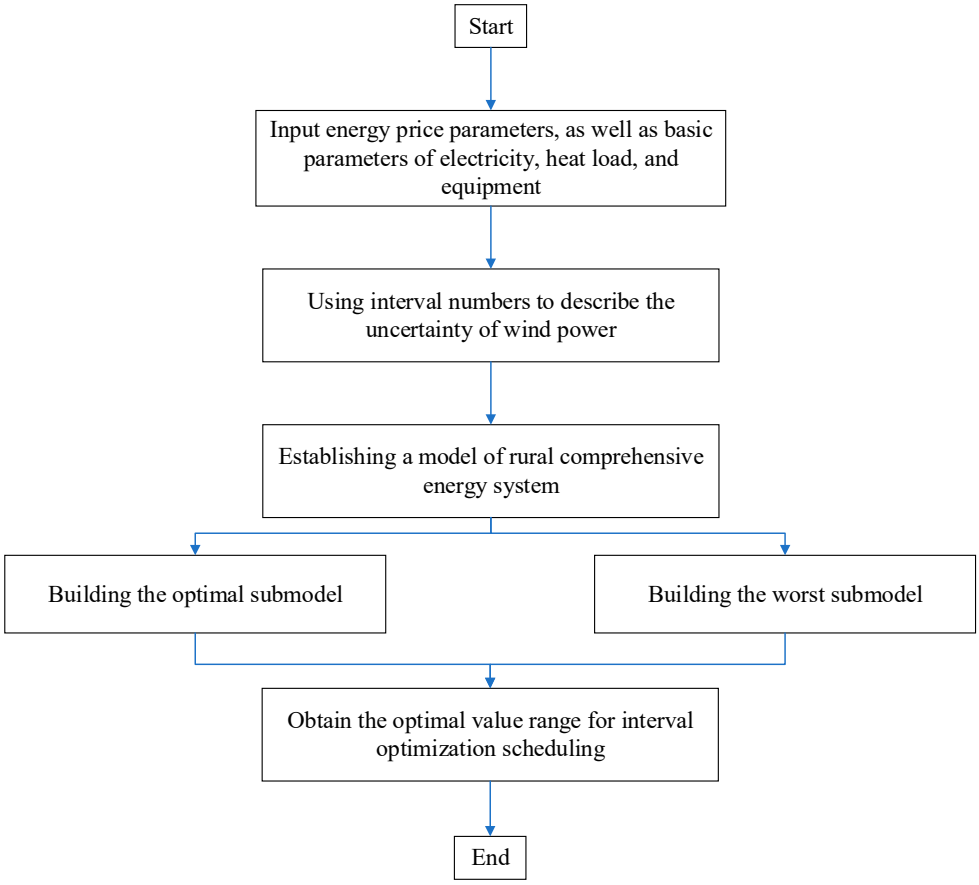


Figure 2. Interval linear optimization algorithm process.

5. Analysis of Calculation Cases

5.1. Basic Settings

In this paper, an integrated rural energy system in Northeast China is used as an example. Comprehensive Refs. [13,29,30] with certain modifications, the device parameters are obtained as in Table 1. The electricity price and the WP prediction interval are shown in Figures 3 and 4.

Table 1. Equipment parameters.

BD	$V_{mg} = 500,\ \eta_{AD} = 0.95$
MT	$P_{\min}^{MT} = 63,\ P_{\max}^{MT} = 318,\ \eta_{MT,e} = 0.35,\ \eta_{MT,h} = 1.5$
EL	$P_{\min}^{EL} = 0,\ P_{\max}^{EL} = 308,\ \eta_{EL} = 0.85$
HP	$P_{\min}^{HP} = 43,\ P_{\max}^{HP} = 213,\ \eta_{HP} = 3.5$
BST	$V_{BST} = 153\ \mathrm{m}^3,\ \eta_{BST} = 0.95$
HST	$V_{HST} = 146\ \mathrm{m}^3,\ \eta_{HST} = 0.95$

5.2. Analysis of Optimization Results

The electric power scheduling results under the optimal scheduling results are shown in Figure 5. the EL makes full use of the redundant WP to produce hydrogen and store it in the HST during the peak WP period 22:00–3:00, while the EL stops producing gas during the low WP period 9:00–21:00, as hydrogen production is no longer economical. The thermal power scheduling results are shown in Figure 6, where the BD stores excess heat during the peak HP output time period of 2:00–8:00 and emits heat to satisfy the heat load from 16:00–21:00, achieving energy time-shifting while reducing HP power consumption.

The BD absorbs more heat than it gives out to make up for the heat lost to the outside world, thus maintaining the fermentation temperature.

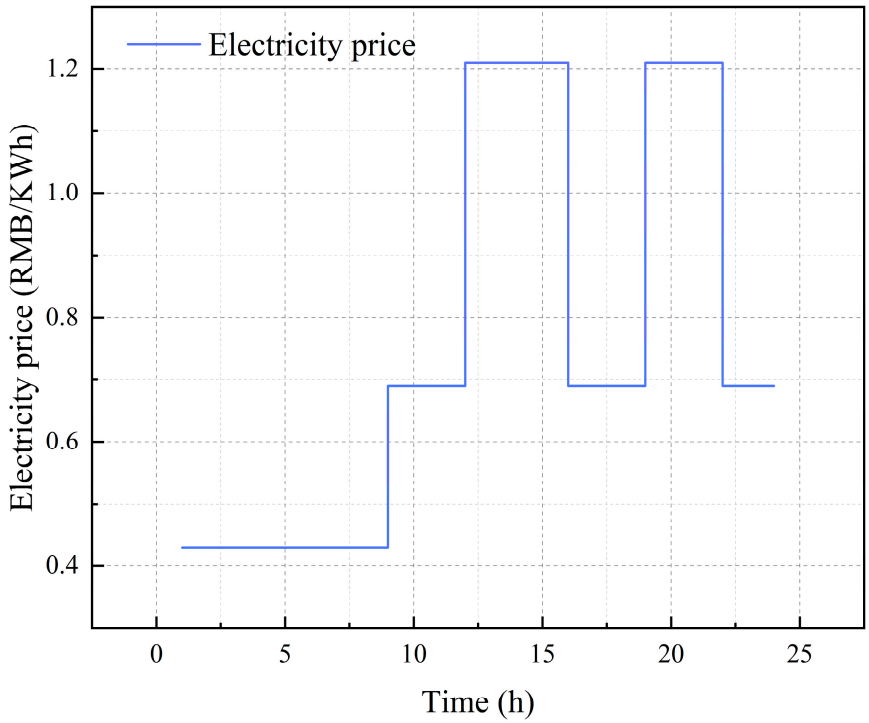


Figure 3. Electricity price.

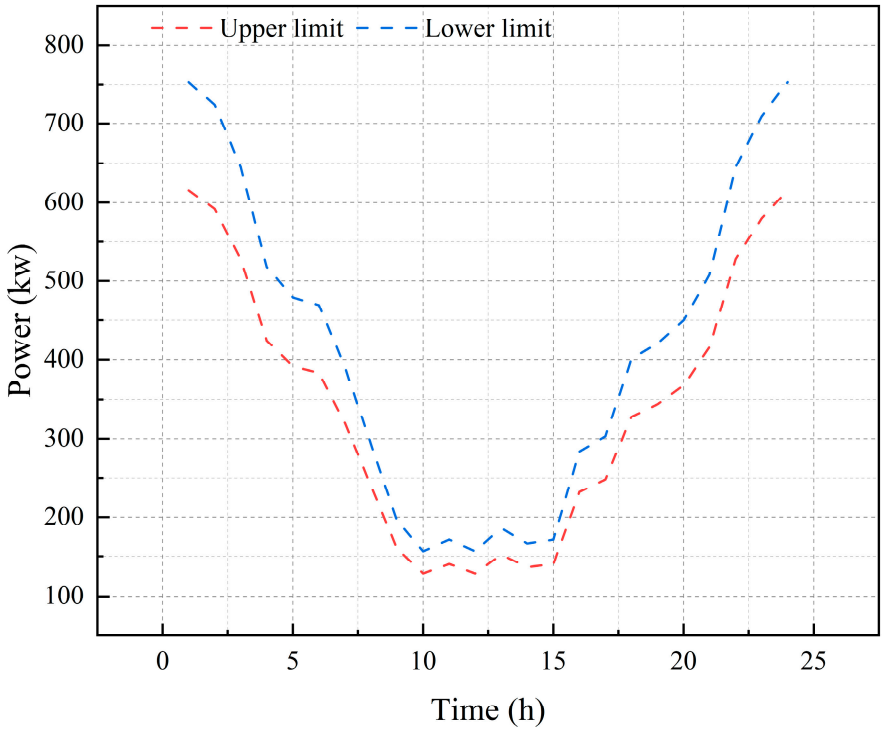


Figure 4. WP prediction interval.

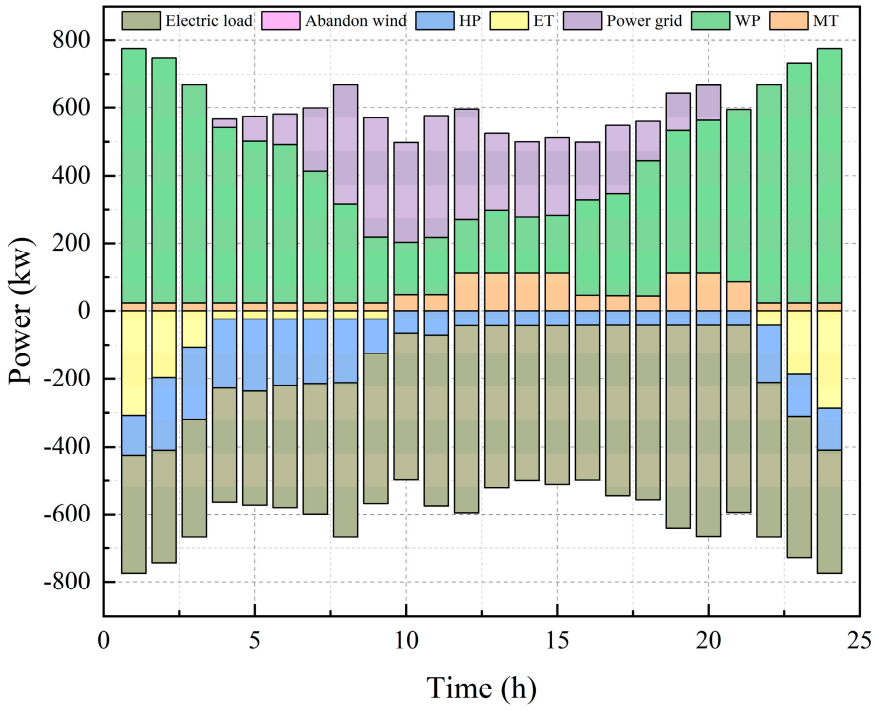


Figure 5. Electric power balance.

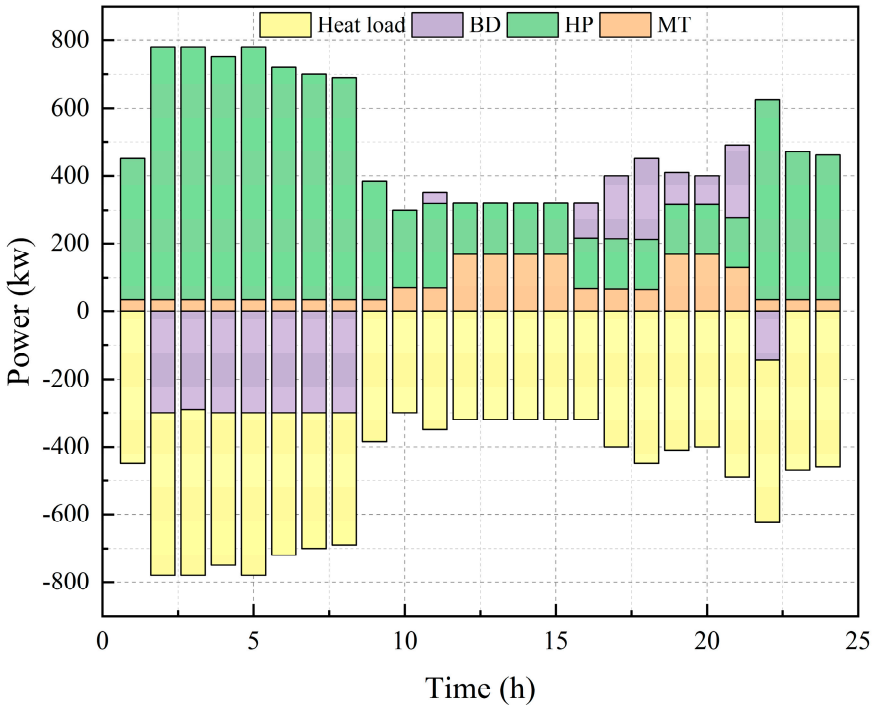


Figure 6. Thermal power balance.

The gas production rate of the EL and BD and the temperature change curve of BD are shown in Figure 7, which maintains a certain gas production rate due to the heat absorbed from the system, similar results were obtained with the ref (Li et al., 2020 [12]). The amount of biogas and hydrogen entering the MT during the time period t is shown in Figure 8. During the periods of higher electricity price, 12:00–15:00 and 19:00–20:00, the BST and HST are discharged, and the MT reaches the maximum gas intake to meet the electrical load of the system.

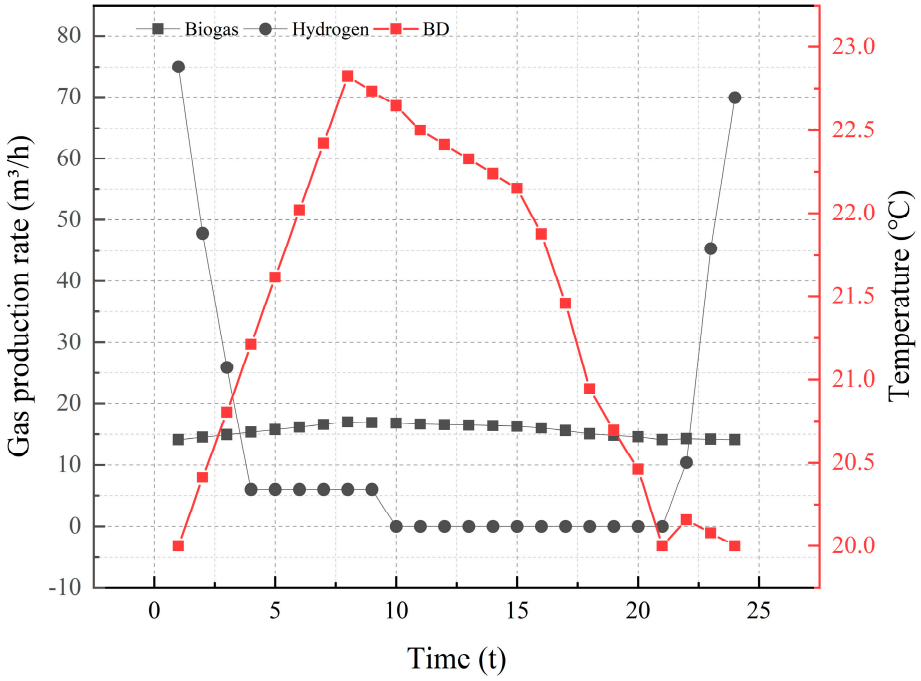


Figure 7. Gas production rate and temperature.

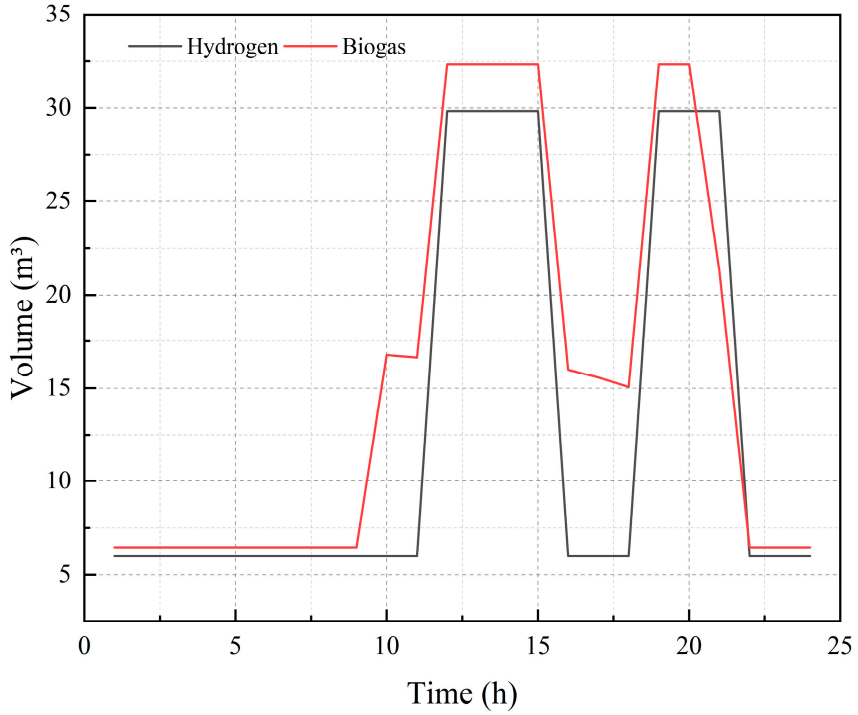


Figure 8. Results of biogas hydrogen blending.

5.3. Scheduling Results for Different Scenarios

For comparative analysis, the following scenarios are set up:

Case 1: Without considering the strategy proposed in this paper, the system considers the uncertainty of WP to be 10%.

Case 2: Without considering the strategy proposed in this paper, the system adds a thermal storage tank and a battery, both with a capacity of 500 kw, and the uncertainty of WP is considered to be 10%.

Case 3: Without considering the strategy proposed in this paper, the system adds a thermal storage tank and a battery, both with a capacity of 1000 kw, and the uncertainty of WP is considered to be 10%.

Case 4: Without considering the strategy proposed in this paper, the system adds a thermal storage tank and a battery, both with a capacity of 1500 kw, and the uncertainty of WP is considered to be 10%.

Case 5: Consider the strategy proposed in this paper and consider the uncertainty of 10% for WP.

The charging and discharging situation of the battery and heat storage pool under the optimal scheduling of Case 2–Case 4 is shown in Figure 9. By absorbing energy during the time when electricity prices are low and releasing it during the time when electricity prices are high, batteries and thermal storage cells can time-shift energy, reduce the cost of purchasing electricity, and increase the utilization of WP.

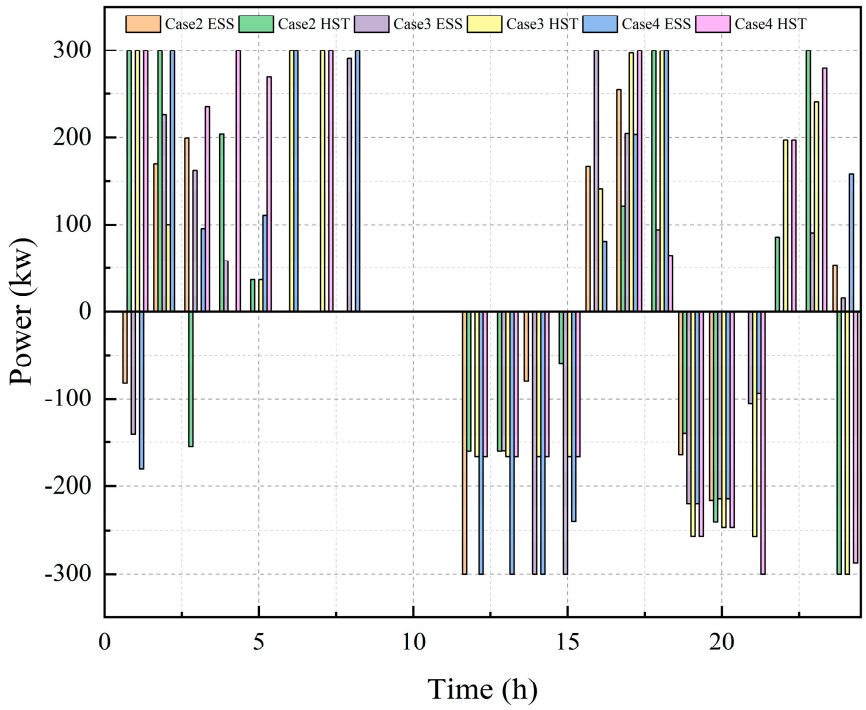


Figure 9. Energy storage equipment status.

The total cost range under different scenarios of cost scheduling are shown in Table 2. Case 2, Case 3, and Case 4 are able to consume the WP and reduce the power purchase due to the addition of energy storage, and the upper and lower limits of the total cost range decrease with the increase in energy storage capacity, Case 2, Case 3, and Case 4 have 22.4%, 31.1%, and 37.3% lower total cost under optimal dispatch compared with Case 1, but the system wind abandonment is not significantly reduced due to the upper limit of energy storage charging and discharging. Case 5 does not have wind abandonment, and the total cost under optimal dispatch is 3.8–22.3% lower than Case 2, Case 3, and Case 4, but the power purchase cost is higher than that of Case 4, and the radius of the interval is the largest, and it is no longer economical compared with Case 4 under the worst dispatch because the addition of EL has certain energy loss and the system economy is limited by the WP output. Compared to the ref (Liu et al., 2022 [22]) that only considers the worst-case scenario, the interval optimization adopted in this article can well reflect the impact of uncertainty.

Table 2. Cost scheduling results.

Scenarios	Total Cost (¥)	Cost of Electricity Purchase (¥)	Wind Abandonment Cost (¥)
Case1	[5923.8, 5944.1]	[4370.6, 5197.1]	[453.6, 1223.7]
Case2	[4595.6, 5055.2]	[3580.3, 4534.8]	[223.7, 682.1]
Case3	[4079.7, 4552.4]	[3080.4, 4039.2]	[216.1, 665.5]
Case4	[3713.1, 4234.2]	[2741.3, 3686.6]	[250.4, 637.9]
Case5	[3571.3, 4599.5]	[2818.8, 3917.1]	0

The degree of uncertainty has a significant effect on interval optimization. The maximum error of the daily WP prediction curve is specified to be no more than 20%. The expected total cost of each scenario under different degrees of certainty is shown in Figure 10. With the increase in uncertainty, the system cost gradually increases incrementally, and when the uncertainty degree is greater than 10%, the system cost growth rate becomes larger, and the dependence of the system on the superior grid increases. Overall, if the uncertainty is below 15%, Case 5 is more economical than Case 1, Case 2, Case 3, and Case 4. If the uncertainty is above 15%, Case 5 is the most economical.

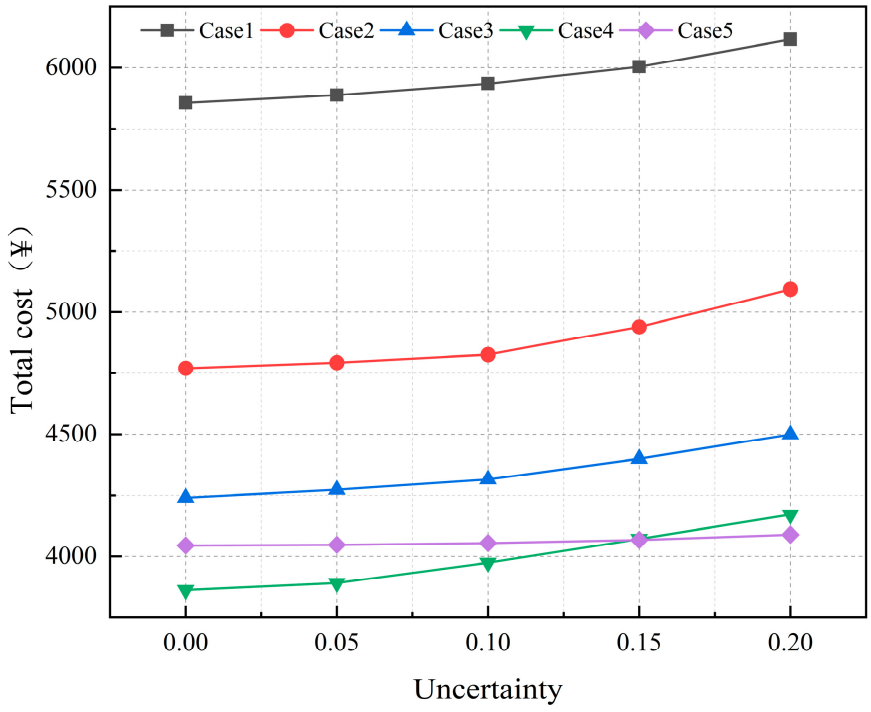


Figure 10. Total cost under uncertainty.

5.4. Sensitivity Analysis

The changes in system costs under uncertainty in electricity prices, gas production, and biomass prices are shown in Figure 11. From the results, it can be found that the total cost is linearly correlated with electricity price, gas production, and biomass price, and the system sensitivity is higher for electricity price, followed by gas production and biomass price. The radius of the interval becomes larger as the degree of uncertainty increases, but the midpoint of the total cost range in these three cases is the same, which means that they only affect the operational costs of the system and have a limited impact on the operational decisions of the system.

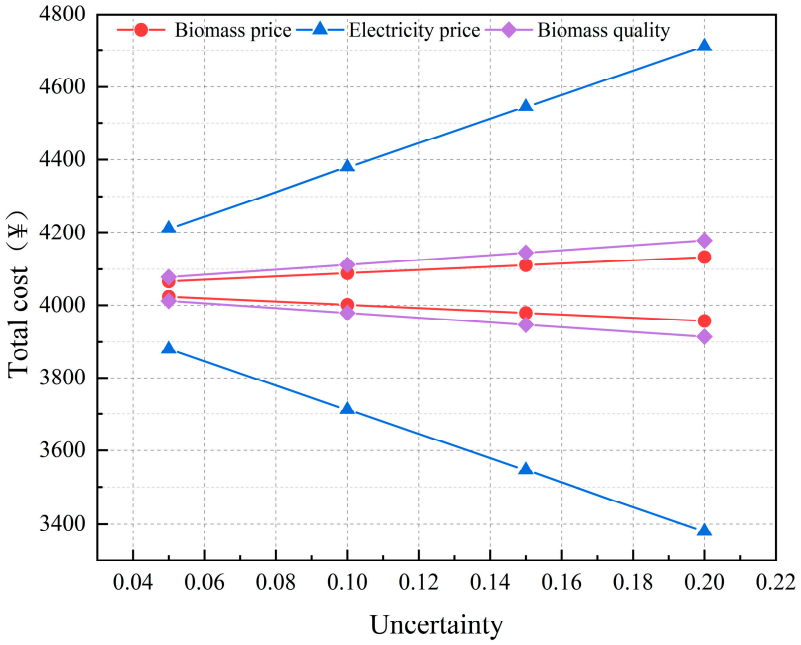


Figure 11. Total cost under different factors.

6. Conclusions

In this paper, we propose a scheduling strategy for an integrated rural energy system considering biogas hydrogenation, expressing the uncertainty of WP in terms of interval numbers and transforming it into a mixed-integer linear model solution using interval optimization, and the results of the example draw the following conclusions.

(1) The uncertainty of WP can be better handled by using interval mathematics to represent the uncertainty of WP, and the obtained results can show the influence of uncertainty on the system more realistically.
(2) The paper proposes a strategy that can significantly maintain the fermentation temperature of the BD in winter and improve the utilization of biomass, and the inclusion of EL can significantly reduce the abandoned wind rate, promote the consumption of WP and improve the utilization of renewable energy.
(3) Within 10% WP uncertainty, the strategy proposed in this paper has better economy and stability compared to peaking with storage batteries and thermal storage pools both with capacities of 1500 kw or less, but the radius of the interval is the largest. In terms of uncertainty, the fluctuation of electricity prices has a greater impact on the system.
(4) The model proposed in this paper can provide some considerations for the optimization of integrated rural electric and thermal energy systems. This paper mainly concerns the complementary characteristics of renewable energy sources, and subsequent studies will incorporate the equipment capacity into the planning.

Author Contributions: Conceptualization, H.L.; Writing—original draft, S.Y.; Writing—review & editing, M.Z. All authors have read and agreed to the published version of the manuscript.

Funding: This work was supported by the National Natural Science Foundation of China [grant numbers 71963024].

Data Availability Statement: The [DATA TYPE] data used to support the findings of this study are available from the corresponding author upon request.

Conflicts of Interest: The authors declare no conflict of interest.

References

1. Hetland, J.; Yowargana, P.; Leduc, S.; Kraxner, F. Carbon-negative emissions: Systemic impacts of biomass conversion: A case study on CO_2 capture and storage options. *Int. J. Greenh. Gas Control* **2016**, *49*, 330–342. [CrossRef]
2. Sun, R.; Liu, T.; Chen, X.; Yao, L. A biomass-coal co-firing based bi-level optimal approach for carbon emission reduction in China. *J. Clean. Prod.* **2021**, *278*, 123318. [CrossRef]
3. Yang, C.; Kwon, H.; Bang, B.; Jeong, S.; Lee, U. Role of biomass as low-carbon energy source in the era of net zero emissions. *Fuel* **2022**, *328*, 125206. [CrossRef]
4. Zhang, T.; Tan, Y.; Zhang, X. Using a hybrid heating system to increase the biogas production of household digesters in cold areas of China: An experimental study. *Appl. Therm. Eng.* **2016**, *103*, 1299–1311. [CrossRef]
5. Yan, R.; Wang, J.; Huo, S.; Qin, Y.; Zhang, J.; Tang, S.; Wang, Y.; Liu, Y.; Zhou, L. Flexibility improvement and stochastic multi-scenario hybrid optimization for an integrated energy system with high-proportion renewable energy. *Energy* **2023**, *263*, 125779. [CrossRef]
6. Song, Y.; Du, M.; Zhao, W.; Lin, H. A new integrated regulation strategy and modelling for wind turbine with battery energy storage system. *J. Energy Storage* **2023**, *63*, 107111. [CrossRef]
7. Wu, G.; Li, T.; Xu, W.; Xiang, Y.; Su, Y.; Liu, J.; Liu, F. Chance-constrained energy-reserve co-optimization scheduling of wind-photovoltaic-hydrogen integrated energy systems. *Int. J. Hydrogen Energy* **2023**, *48*, 6892–6905. [CrossRef]
8. Karaca, A.E.; Dincer, I.; Nitefor, M. A new renewable energy system integrated with compressed air energy storage and multistage desalination. *Energy* **2023**, *268*, 126723. [CrossRef]
9. Liu, J.; Zhou, Y.; Yang, H.; Wu, H. Net-zero energy management and optimization of commercial building sectors with hybrid renewable energy systems integrated with energy storage of pumped hydro and hydrogen taxis. *Appl. Energy* **2022**, *321*, 119312. [CrossRef]
10. Siddiqui, O.; Dincer, I. Design and analysis of a novel solar-wind based integrated energy system utilizing ammonia for energy storage. *Energy Convers. Manag.* **2019**, *195*, 866–884. [CrossRef]
11. Xu, D.; Yuan, Z.-L.; Bai, Z.; Wu, Z.; Chen, S.; Zhou, M. Optimal operation of geothermal-solar-wind renewables for community multi-energy supplies. *Energy* **2022**, *249*, 123672. [CrossRef]
12. Li, C.; Yang, H.; Shahidehpour, M.; Xu, Z.; Zhou, B.; Cao, Y.; Zeng, L. Optimal Planning of Islanded Integrated Energy System with Solar-Biogas Energy Supply. *IEEE Trans. Sustain. Energy* **2020**, *11*, 2437–2448. [CrossRef]
13. Zhou, B.; Xu, D.; Li, C.; Chung, C.Y.; Cao, Y.; Chan, K.W.; Wu, Q. Optimal Scheduling of Biogas–Solar–Wind Renewable Portfolio for Multicarrier Energy Supplies. *IEEE Trans. Power Syst.* **2018**, *33*, 6229–6239. [CrossRef]
14. Zare, A.D.; Saray, R.K.; Mirmasoumi, S.; Bahlouli, K. Optimization strategies for mixing ratio of biogas and natural gas co-firing in a cogeneration of heat and power cycle. *Energy* **2019**, *181*, 635–644. [CrossRef]
15. Zhao, F.; Li, Y.; Zhou, X.; Wang, D.; Wei, Y.; Li, F. Co-optimization of decarbonized operation of coal-fired power plants and seasonal storage based on green ammonia co-firing. *Appl. Energy* **2023**, *341*, 121140. [CrossRef]
16. Kim, Y.-K.; Kim, J.-H.; Yoo, S.-H. Public perspective on co-firing hydrogen with natural gas in power plants in South Korea. *Int. J. Hydrogen Energy* **2023**, *48*, 4119–4128. [CrossRef]
17. Zhang, Q.; Liu, Y.; Cao, Y.; Li, Z.; Hou, J.; Gou, X. Parametric study and optimization of MEA-based carbon capture for a coal and biomass co-firing power plant. *Renew. Energy* **2023**, *205*, 838–850. [CrossRef]
18. Zeng, L.; Xu, J.; Wu, M.; Tang, J.; Wu, Q.; Wang, Q.; Fan, G. Day-ahead interval optimization for CCHP system considering uncertainty of wind power and PV. *Int. J. Electr. Power Energy Syst.* **2022**, *138*, 107895. [CrossRef]
19. Jiang, T.; Li, X.; Kou, X.; Zhang, R.; Tian, G.; Li, F. Available transfer capability evaluation in electricity-dominated integrated hybrid energy systems with uncertain wind power: An interval optimization solution. *Appl. Energy* **2022**, *314*, 119001. [CrossRef]
20. Liu, X.; Hou, M.; Sun, S.; Wang, J.; Sun, Q.; Dong, C. Multi-time scale optimal scheduling of integrated electricity and district heating systems considering thermal comfort of users: An enhanced-interval optimization method. *Energy* **2022**, *254*, 124311. [CrossRef]
21. Liu, G.; Qin, Z.; Diao, T.; Wang, X.; Wang, P.; Bai, X. Low carbon economic dispatch of biogas-wind-solar renewable energy system based on robust stochastic optimization. *Int. J. Electr. Power Energy Syst.* **2022**, *139*, 108069. [CrossRef]
22. Xiao, H.; Long, F.; Zeng, L.; Zhao, W.; Wang, J.; Li, Y. Optimal scheduling of regional integrated energy system considering multiple uncertainties and integrated demand response. *Electr. Power Syst. Res.* **2023**, *217*, 109169. [CrossRef]
23. Su, X.; Shao, X.; Geng, Y.; Tian, S.; Huang, Y. Optimization of feedstock and insulating strategies to enhance biogas production of solar-assisted biodigester system. *Renew. Energy* **2022**, *197*, 59–68. [CrossRef]
24. Gholamian, E.; Mehr, A.; Yari, M.; Carton, J. Dynamic simulation and techno-economic assessment of hydrogen utilization in dual fuel (Hydrogen/biogas) micro gas turbine systems for a wastewater treatment plant. *Process Saf. Environ. Prot.* **2023**, *169*, 220–237. [CrossRef]
25. Bui, V.G.; Tu Bui, T.M.; Ong, H.C.; Nižetić, S.; Bui, V.H.; Xuan Nguyen, T.T.; Atabani, A.E.; Štěpanec, L.; Phu Pham, L.H.; Hoang, A.T. Optimizing operation parameters of a spark-ignition engine fueled with biogas-hydrogen blend integrated into biomass-solar hybrid renewable energy system. *Energy* **2022**, *252*, 124052. [CrossRef]
26. Bai, L.; Li, F.; Cui, H.; Jiang, T.; Sun, H.; Zhu, J. Interval optimization based operating strategy for gas-electricity integrated energy systems considering demand response and wind uncertainty. *Appl. Energy* **2016**, *167*, 270–279. [CrossRef]

27. O'Shea, R.; Wall, D.M.; Kilgallon, I.; Browne, J.D.; Murphy, J.D. Assessing the total theoretical, and financially viable, resource of biomethane for injection to a natural gas network in a region. *Appl. Energy* **2017**, *188*, 237–256. [CrossRef]
28. Dong, Y.; Zhang, H.; Ma, P.; Wang, C.; Zhou, X. A hybrid robust-interval optimization approach for integrated energy systems planning under uncertainties. *Energy* **2023**, *274*, 127267. [CrossRef]
29. Wu, Q.; Li, C. Modeling and operation optimization of hydrogen-based integrated energy system with refined power-to-gas and carbon-capture-storage technologies under carbon trading. *Energy* **2023**, *270*, 126832. [CrossRef]
30. Wang, L.; Lin, J.; Dong, H.; Wang, Y.; Zeng, M. Demand response comprehensive incentive mechanism-based multi-time scale optimization scheduling for park integrated energy system. *Energy* **2023**, *270*, 126893. [CrossRef]

Disclaimer/Publisher's Note: The statements, opinions and data contained in all publications are solely those of the individual author(s) and contributor(s) and not of MDPI and/or the editor(s). MDPI and/or the editor(s) disclaim responsibility for any injury to people or property resulting from any ideas, methods, instructions or products referred to in the content.